Submitted to Limnology and Oceanography:

Physical and biological processes underlying the sudden appearance of a red-tide surface patch in the nearshore.

Melissa M. Omand,* James J. Leichter, Peter J. S. Franks, R. T. Guza, Andrew J. Lucas, and Falk Feddersen

Scripps Institution of Oceanography, San Diego, California 92093-0209

*Corresponding author: momand@ucsd.edu

Report Documentation Page

Form Approved
OMB No. 0704-0188

1. REPORT DATE	2. REPORT TYPE	3. DATES COVERED
2010		**00-00-2010 to 00-00-2010**

4. TITLE AND SUBTITLE	5a. CONTRACT NUMBER
Physical and biological processes underlying the sudden appearance of a red-tide surface patch in the nearshore.	5b. GRANT NUMBER
	5c. PROGRAM ELEMENT NUMBER
6. AUTHOR(S)	5d. PROJECT NUMBER
	5e. TASK NUMBER
	5f. WORK UNIT NUMBER
7. PERFORMING ORGANIZATION NAME(S) AND ADDRESS(ES) **Scripps Institution of Oceanography,San Diego,CA,92093-0209**	8. PERFORMING ORGANIZATION REPORT NUMBER
9. SPONSORING/MONITORING AGENCY NAME(S) AND ADDRESS(ES)	10. SPONSOR/MONITOR'S ACRONYM(S)
	11. SPONSOR/MONITOR'S REPORT NUMBER(S)

12. DISTRIBUTION/AVAILABILITY STATEMENT
Approved for public release; distribution unlimited

13. SUPPLEMENTARY NOTES

14. ABSTRACT

15. SUBJECT TERMS

16. SECURITY CLASSIFICATION OF:			17. LIMITATION OF ABSTRACT	18. NUMBER OF PAGES	19a. NAME OF RESPONSIBLE PERSON
a. REPORT	b. ABSTRACT	c. THIS PAGE			
unclassified	**unclassified**	**unclassified**	**Same as Report (SAR)**	**46**	

Acknowledgments

B. Woodward, B. Boyd, K. Smith, D. Darnell, I. Nagy, D. Clark, M. Rippy, M. McKenna, and D. Michrowski assisted in collecting field observations. H. Mcclendon counted and identified the phytoplankton samples. The Golden West College Observatory collected surface irradiance data. These observations were obtained within the framework of the larger Southern California Coastal Ocean Observing System (SCCOOS) and United States Geological Survey (USGS) programs at Huntington Beach. George Robertson, Marlene Noble, Uwe Send, Steve Weisberg are thanked for their cooperation and assistance. California Sea Grant, NOAA, California Coastal Conservancy, NSF and ONR supported this research. Sea Grant support was through the California Sea Grant College Program Project #R/CZ-196, through NOAA's National Sea Grant College Program, U.S. Dept. of Commerce. The statements, findings, conclusions and recommendations are those of the authors and do not necessarily reflect the views of California Sea Grant or the U.S. Dept. of Commerce.

Abstract

The factors contributing to the timing and intensity of phytoplankton blooms ("red tides") in very shallow water are poorly understood. Here, the sudden and brief (3 h) appearance at the surface of an alongshore-parallel band of red tide is described. The bloom, near Huntington Beach CA, was dominated by the locally common red-tide forming dinoflagellate *Lingulodinium polyedrum* (F. Stein). Surface chlorophyll-a (Chl *a*) and temperature (*T*) were mapped with a novel GPS-tracked jetski. The surface red-tide band, with maximum Chl *a* ~7 μgL^{-1}, was visible for more than 3 h, was located 500 m from shore (~8 m water depth), was ~200 m wide and extended ~1 km alongshore. The subsurface bloom, with maximum Chl *a* > 30 μgL^{-1}, developed farther offshore, near the 17 °C isotherm over 4-7 days prior to the surface appearance. A few hours before the surface band appeared, an intense Chl *a* patch was observed in 13 m total depth in the mid-water column trough of a shoreward-propagating supertidal internal wave. The Chl *a* patch intensification was consistent with dinoflagellate vertical swimming interacting with the wave-driven circulation. In shallow water (<12 m depth), vertical mixing, attributed to internal wave breaking, brought the Chl *a* patch to the surface. Warm water in very shallow water (depth < 5 m) apparently blocked the Chl *a* patch from entering the surfzone. These observations highlight the role of small-scale physical and biological processes in determining the spatial and temporal characteristics of nearshore red tide blooms.

Introduction

Intense phytoplankton blooms (“red tides”) and harmful algal blooms (HABs) in the nearshore (<15 m depth), incur losses of millions of dollars annually to aquaculture (Alonso-Rodriguez and Paez-Osuna, 2003), threaten marine mammal and human health (Anderson, 1997), and inhibit beach recreation (Backer et al. 2003). Nearshore red tides are difficult to predict and monitor (Anderson, 1997), in part, because phytoplankton are transported, mixed and concentrated by a range of physical processes, including upwelling (e.g., Smith et al. 1983), winds (e.g., Keafer et al. 2005), alongshore plumes (e.g., Franks and Anderson, 1992), internal tidal bores (e.g., Leichter et al. 1998), internal waves (Lenert-Cody and Franks, 2002) and tidal currents and stirring (e.g., Cloern and Dufford, 2005). In the surfzone (within the shallow region of surface wave-breaking), currents (Campbell and Bate, 1988) and species-specific behavior (Talbot and Bate, 1986) appear to control the distributions of several sand-dwelling diatom species. This broad range of mechanisms can create surface patches of red tide organisms that may be much smaller (meters) and shorter in duration (hours, e.g., Franks, 1997) than the scales of the growth and decline of the bloom itself (kilometers and weeks, e.g., Weiters et al. 2003).

The impact of a red tide on the nearshore depends on the local bloom intensity and duration. Mussels briefly exposed to high doses of HAB toxins may surpass quarantine limits within one hour (Bricelj et al. 1990), indicating that sudden changes in red tide concentration and distribution may carry important consequences for mussel health. “Cryptic" blooms may develop as thin subsurface layers (McManus et al. 2008), with no (or limited) surface expression and therefore invisible to satellites and visual inspection. *In situ* sampling, including subsurface waters, at scales fine enough to resolve

transient and subsurface Chlorophyll *a* (Chl *a*) or HAB layers is critical for effective monitoring.

Many marine phytoplankton are motile, and capable of maintaining position in the water column position despite negatively buoyant cell bodies (Cox, 1980). A combination of motility and convergent advection may lead to accumulation of phytoplankton at fronts (Franks, 1992) or in internal wave troughs (Lennert-Cody and Franks, 1999). Swimming has been implicated in the accumulation of larvae at internal tidal fronts (e.g., Clancy and Epifanio, 1989) and shoreward-propagating bores (e.g., Pineda, 1999). However, the relative importance of swimming and physical mechanisms in concentrating and transporting phytoplankton to the nearshore is poorly understood.

In this paper, biological and physical observations of a nearshore red tide are presented from Fall 2006 as part of the Huntington Beach experiment (HB06). This site was selected in part because of chronic beach water quality problems (Boehm et al. 2002a). Previous studies include investigations of the internal-tide driven cross-shore transport of sewage effluent (Boehm et al. 2002b), subthermocline water, and suspended or dissolved material (Noble et al. 2009). Subtidal internal bores (with durations of 2-5 hrs) may also be responsible for cross-shore sediment transport (Noble and Xu, 2003). This is the first study to explore the high spatial and temporally resolved patterns and transport of a red tide at this site. Santoro et al. (2010) use Sea-viewing Wide Field-of-view Sensor (SeaWiFS) to contrast red tide blooms in 2005 (an anomalous year with an intense 6-month bloom) and 2006 (with comparatively low SeaWIFS Chl *a*) with a focus on Huntington Beach. However, satellite measurements cannot detect subsurface, short-time, or small-scale blooms.

Here, the sudden surface appearance of a subsurface “cryptic bloom” of the dinoflagellate *Lingulodinium polyedrum* is described. The surface expression of the bloom, visible from the beach as a brown streak ~1 km from shore and extending >1 km alongshore (Fig. 1) developed over the course of a few hours on 12 Oct 2006. Intensive and unique biophysical observations with high temporal and spatial resolution, spanning 4 km cross-shore, from the surfzone to 25 m total depth (Fig. 2), indicate that the bloom developed in the nearshore, within a subsurface layer over about 4 to 7 days. An intense subsurface Chl *a* patch formed within a shoreward-propagating internal wave trough, consistent with models of depth-keeping swimming behavior in the internal wave-induced circulation. Internal wave breaking in shallow water (depth < 12 m) is implicated in the vertical spreading of the intense patch, forming the visible band of surface Chl *a* just seaward of the surfzone, without entering the surfzone.

Methods

The nearshore HB06 field experiment was conducted at Huntington Beach, CA from 15 Sept. to 17 Oct 2006, within the framework of the larger scale Southern California Coastal Ocean Observing System (SCCOOS) and United States Geological Survey (USGS) programs. Here the focus is on a few days of HB06 observations, spanning 0.5 km alongshore (y) and 4 km offshore (x) to 25 m depth (Fig. 2). The mean (tidally-averaged) water depth is denoted as H, and the vertical coordinate z is positive upward, with $z = 0$ m at the tidally averaged surface.

Jetski surface maps and CTD+Chl a Casts

Quasi-synoptic maps of near-surface Chl *a*, turbidity and temperature (*T*) were constructed at 45 min intervals between 1200 and 1500 h from data acquired by a flow-through sampling system mounted on a GPS-tracked jetski (Clark et al. 2009). The jetski was driven on 1 km long cross-shore transects between the shoreline and ~12 m depth with 8 transects distributed over 600 m alongshore (dashed box in Fig. 2a). CTD (Seabird 19) and flow-through Chl *a* fluorometer (WET Labs WETStar) casts were made at stations on a single cross-shore transect. Cross-shore transects were made between H = 40 m to H = 5 m (spanning ~6 km) from 0900 to 1130 h once per day on various days throughout HB06. In addition, on 12 Oct at 45 min intervals between H = 13 m to H = 4 m from 1200 to 1500 h. Vertical profile data were averaged into 1 m vertical bins. Jetski-derived surface transects (x,y) and CTD+ Chl *a* -derived cross-shore transects (x,z) were objectively mapped with a skill threshold of 0.95 and a signal-to-noise ratio of 0.9 (Bretherton et al. 1976).

Moorings

Moorings were deployed on a 4 km long cross-shore transect at mean (tidally-averaged) water depths H = 8, 15, 18 and 24 m (M8, M15, M18, M24 in Fig. 2) and instrumented with 4 to 6 Star-Oddi (T only) or Sea Bird MicroCAT (S and T) instruments sampling at 3 min intervals. A wirewalker, a wave-driven vertically profiling platform (Rainville and Pinkel, 2001), was deployed at H = 13 m (M13 in Fig. 2), and instrumented with a CTD (Seabird 49, sample rate 16 Hz) and Chl *a* fluorometer (WET Labs ECO Triplet, sample rate 16 Hz). Vertical CTD+ Chl *a* M13 profiles were completed approximately every 2 min; data were averaged every 0.1 m in z and

interpolated onto regular 4 min intervals. Cross-shore (u) and alongshore (v) currents measured with acoustic Doppler current profilers (ADCPs) deployed at the base of moorings M13 (600 kHz), M15 (600 kHz) and M18 (600 kHz) were averaged at 6 min intervals with 1 m vertical bins. A bottom-mounted Nortek Aquadopp at M8 (2000 kHz) sampled every 2.5 min with 0.5 m vertical bins.

Surfzone frames

Fixed frames with acoustic doppler velocimeters, pressure and temperature sensors (sampled at 8 Hz, 8 Hz and 0.2 Hz respectively) were deployed on a cross-shore transect spanning 160 m from near the shoreline to 4 m water depth. In addition, WET Labs ECO Triplet fluorometers measuring Chl *a* (sampled at 0.25 Hz) were repeatedly deployed for 72 h periods on a frame from within (M1.5, H = 1.5 m) and seaward (M4, H = 4 m) of the surfzone (inset in Fig. 2b), facing 30 degrees from downward, nominally 0.5 m above the seafloor. A correction for data biases induced by the turbid surfzone conditions was applied the ECO Triplets (Omand et al. 2009).

Water Samples

At most casts, water samples (for Chl *a* analysis and phytoplankton cell counts and identification) were collected near the bottom with a messenger-tripped Niskin bottle mounted 1 m above the CTD, and at the surface by hand. Water samples were also collected near the surface every 20 min on Oct 12 from 900 to 1500 h near M1.5 and M4. Samples for taxonomic identification were preserved by transferring 100 ml of raw seawater to a glass Wheaton bottle and combined with 10 ml buffered 37% Formaldehyde. The preserved samples were analyzed with the Utermöhl settling method

(Utermöhl, 1958) and inspected at 16X magnification under a light microscope. All visible cells (>5 μm) were enumerated and identified to a genus or species level when possible.

Nonphotochemical quenching correction

Nonphotochemical quenching (NPQ) reduces Chl *a* fluorescence in high light conditions (e.g., Kiefer 1973, Falkowski and Raven 1997, Muller et al. 2001). NPQ corrections, derived from continuous profiles of Chl *a* at M13 (Fig.2) and surface irradiance (measured with a Davis Vantage Pro Plus cosine pyranometer), were applied to all *in situ* Chl *a* measurements (see the Web Appendix M13w.aslo.org/lo/toc/vol_xx/issue_x/xxxxa1.pdf). The NPQ correction is small and does not affect the overall patterns and conclusions.

Results

The sudden surface appearance of a nearshore, dense red-tide patch is described, using physical and biological data with uniquely high spatial and temporal resolution. Nearshore ($H < 15$ m) Chl *a* was generally low on 5 Oct (maximum 4.5 μgL^{-1}, Fig. 3a) and reached 13 μgL^{-1} on 8 Oct and 9 Oct in a subsurface layer between the 16 and 17 °C isotherms (Fig. 3b,c). Maximum Chl *a* peaked above 34 μgL^{-1} on 12 Oct (Fig. 3d), and decreased to 12 μgL^{-1} on 16 Oct (Fig. 3e). Offshore ($15 \text{ m} < H < 50$ m) Chl *a* within the subsurface layer also increased, though less intensely, from a Chl *a* maximum of 6 μgL^{-1} on 5 Oct to 10 μgL^{-1} on 12 Oct. Glider surveys conducted approximately 1-10 km offshore, concurrently with HB06, also indicate an increase of mean subsurface Chl *a* between 29 Sept and 16 Oct (Todd et al. 2009).

Conditions on 12 Oct were typical of a fall day at Huntington Beach; winds were weak, blowing slightly offshore in the morning with a northwest 3 ms^{-1} breeze in the afternoon. The surface water temperature was approximately 17.5 °C, dropping to 14 °C at the base of the thermocline at ~ 20 m (Fig. 3d). Offshore (H > 15 m depth), a deep Chl *a* maximum (DCM) layer of 10 μgL^{-1} Chl *a* lay between the 14 and 16 °C isotherms. In the nearshore (H < 15 m depth) an intense patch of Chl *a* was observed between the 16 and 17 °C isotherms (Fig. 3d). Nearshore and offshore phytoplankton taxonomic composition (Table 1) was strikingly different. The nearshore was dominated by a near monoculture of dinoflagellates (> 70% *Lingulodinium polyedrum*) while offshore waters contained a greater diversity of genera, dominated by diatoms from the genera *Asterionella* and *Chaetoceros*. *L. polyedrum* were also the dominant nearshore cells on 8, 9, and 16 Oct. The nearshore increase in Chl *a* between 5 - 12 Oct corresponds to a Chl *a*-specific growth rate of ~ 0.3 d^{-1}. This growth rate, reasonable for *L. polyedrum* (e.g., Sullivan and Swift, 2003), suggests that the monotonic increase in subsurface Chl *a* concentrations was largely generated by local growth of this species.

Five CTD+ Chl *a* cross-shore transects and near-synoptic jetski surveys of surface Chl *a* and *T* were conducted at 45 min intervals between 1200 and 1500 h in the nearshore region inshore of M13 (Fig. 2). At 1200 h, a high Chl *a* concentration (up to 39 μgL^{-1}) layer was located ~ 5 m below the surface (Fig. 4a). Surface Chl *a* and temperature were spatially homogeneous at 3 μgL^{-1} and 17.7 °C, respectively (Fig. 4a,b). The hourly-averaged cross-shore currents were directed ~0.03 ms^{-1} onshore near the surface and offshore near the seafloor. The surfzone alongshore current was 0.15 ms^{-1} northward. By 1245 h, a small (~10 m cross- and alongshore) patch of approximately 4 μgL^{-1} Chl *a* appeared at the surface with slightly cooler, 17.5 °C water (Fig. 4c,d), and the

subsurface high-concentration Chl *a* patch moved inshore (between 300 < x < 600 m). The patch center lay just below the 17 °C isotherm.

At 1330 h (Fig. 4e,f), a 5 μgL^{-1} Chl *a* patch had further emerged at the surface near x = 400 m in 17.5 °C water, spanning 100 m across shore and 250 m alongshore. The near-surfzone region (x < 150 m) had warmed to 18 °C. The subsurface, concentrated Chl *a* patch was centered on the 17 °C isotherm and increased in thickness. At 1415 h, the surface Chl *a* patch was developed, with a 7 μgL^{-1} maximum, a cross-shore span of about 200 m (Fig. 4g) and visually estimated alongshore length ~ 1 km. The near-surfzone region continued to warm and the colder (< 17 °C) surface water at x > 500 m receded offshore (Fig. 4h). The Chl *a* patch continued to spread vertically into warmer 17.5 to 18 °C water. Later at 1500 h, the surface Chl *a* patch had advected slightly offshore with the < 17.5 °C water (Fig. 4i,j).

Stages of the surface red tide patch formation

The sudden appearance of the red tide at the surface was the culmination of several physical-biological processes. Shoreward propagation of an internal wave trough, advection of a subsurface red tide layer, local formation of a dense Chl *a* patch within the trough, vertical patch spreading, all contributed to the appearance of the surface Chl *a* band. The observations underlying each stage, and the subsequent disappearance from very shallow water, are described.

Shoreward propagation of a supertidal internal wave

On 12 Oct. between 0000 (midnight) and 0300 h, mid-water column isotherms at M24 moved upwards about 5 m, followed by an approximately 7 m drop into an internal

wave trough at 0500 h (star, Fig. 5a). The shoreward-propagating supertidal internal wave (sIW) trough subsequently passed M18 and M15, reaching M13 at 1100 h (black stars, Fig. 5b,c,d). At M8 (H = 7.8 m), the sIW was obscured with no obvious isotherm trough (Fig. 5e).

The sIW propagation time-lag Δt, the time between arrivals of the sIW trough (isotherm minima, black stars, Fig. 5) is estimated for adjacent moorings (not including M8). These Δt give the maximum correlation ($r^2 > 0.63$, $p < 0.001$, Table 2) between mid-water column isotherm depth anomalies (e.g. Lerczak, 2000) over a 15 h period (from 0000 to 1500 h) that includes the sIW trough (Fig. 6a). The observed cross-shore phase velocity $C_p = \Delta x/\Delta t$, where Δx is the cross-shore separation between adjacent moorings decreased from 0.16 ms^{-1} between M24 and M18 to 0.12 ms^{-1} between M15 (black points, Fig. 6b). With constant buoyancy (N) and wave (ω) frequencies, the theoretical phase speed (C_p) for a cross-shore propagating, mode 1, internal wave (e.g., Gill, 1982)

$$C_p = \frac{H}{\pi}\sqrt{N^2 - \omega^2}, \qquad (1)$$

depends linearly on the depth H. C_p (1) is estimated using the vertically-averaged N (estimated from dT/dz adjusted to density), and the mean H, of adjacent moorings. The buoyancy frequency N (~ 0.02 s^{-1}) was large compared to ω, so theoretical C_p was insensitive to the choice of ω (C_p varied by < 1% for wave periods between 2 and 12 hrs: a nominal period of 2 hrs was used). The observed and theoretical (1) C_p were similar (compare gray and black curves Fig. 6b). The sIW propagated coherently about 3km onshore between M24 and M13 and the observed C_p decreased with decreasing depth, as often observed for supertidal internal waves on the Southern California shelf (e.g., Winant, 1974; Winant and Olsen, 1976; Lerczak, 2000; Johnson et al. 2001).

Advection of the subsurface red tide layer and dense Chl a patch

On 11 - 12 Oct at M13 (H = 13 m), the tide varied ± 1 m (Fig. 7a). The cross-shore currents at M13 were dominated by baroclinic modes with both diurnal and semidiurnal variability (Fig. 7b), consistent with prior studies at this location (Boehm et al. 2002; Noble et al. 2009). The subsurface elevated Chl *a* (~10-20 μgL^{-1}, Fig. 7c) layer repeatedly shoaled from near-bottom to near-surface and back down. The Chl *a* layer generally followed the 16.0 - 17.0 °C isotherms (black contours in Fig. 7c) throughout the diurnal cycle, except for a few hours after the 17.5 °C isotherm descended, leaving a near-surface (z > -5 m), 5 μgL^{-1} Chl *a* band above the 17.5° C isotherm (e.g., at t = -32, -8 and 14 h in Fig. 7c).

At M13 between 1000 and 1200 h on 12 Oct, the *L. polyedrum* dominated Chl *a* patch (Fig. 3d), maximum concentrations was 31 μgL^{-1} between 5 and 7 m below the surface, at the 17.0 °C isotherm (Fig. 8). The onshore currents (approximately 0.05 ms^{-1} between 1000 and 1200 h) within the layer (-7 < z < -5 m) transported the patch shoreward. Based on the onshore u over the 2 hr M13 patch duration, the high concentration subsurface Chl *a* patch was estimated to be 200 m wide across-shore, consistent with the jetski observations at the surface (Fig. 6). Below the patch (z < -9 m, Fig. 8), Chl *a* fell to 6 μgL^{-1}, and the cross-shore currents u were directed offshore. After 1200 h, the upper layer Chl *a* concentrations were reduced to around 10 μgL^{-1} as u in that layer weakened (< 0.01 ms^{-1} onshore). Between 1400 and 1600 h, the lower layer (z < -7m) contained elevated Chl *a* that was transported offshore past M13 by offshore u (Fig. 8). At 1600 h, the upper layer (z > -7 m) currents had become offshore directed, transporting a surface patch of > 4 μgL^{-1} Chl *a* seaward. By 1800 h, Chl *a* had decreased to moderate (5 μgL^{-1}) levels throughout most of the water column. At 2000 h, a second

pulse of near-bed elevated Chl *a* (near 15 μgL^{-1}) was advected shoreward as the 17.0 °C isotherm rose to z = -8 m.

Formation of the dense subsurface Chl a patch within an internal wave trough

Phytoplankton advection by IWs in combination with depth-keeping swimming behavior may locally enhance Chl *a* above wave troughs as the isotherm depth beneath the surface Δz increases (Lennert-Cody and Franks 1999, 2002). Evidence of systematically elevated Chl *a* within the sIW-associated isotherm troughs is presented, qualitatively consistent with internal wave-induced convergence and phytoplankton depth-keeping.

At M13 on 12 Oct, Chl *a* in the sIW trough (black star, Fig. 5d), was maximum (31 μgL^{-1}) and nearly triple the mean concentration (11.5 μgL^{-1}) bordering the 17.0 °C isotherm. Chl *a*, vertically-averaged between the 17.0 °C isotherm and the surface (solid black curve in Fig. 5d) and the isotherm separation Δz were significantly positively correlated (Fig. 9a). Mean Chl *a* was maximal where the isotherms were the deepest. In contrast, T, vertically averaged between the 17.0 °C isotherm and the surface, was uncorrelated with Δz. The linear relationship between the vertically averaged Chl *a* and Δz and the absence of a T-Δz relationship do not depend on the choice of isotherm within the range 16.5 to 17.2 ^{o}C, associated with the sIW. Although NPQ can induce apparent along-isotherm Chl *a* variability on a depth-varying isotherm, the maximum NPQ correction (see Web Appendix) for Chl *a* on the 17.0 °C isotherm is 9%, far smaller than the observed Chl *a* variability.

Vertical spreading of the dense subsurface Chl a patch

The surface Chl *a* patch appeared around 1245 h on an isotherm warmer (T = 17.5 °C) than the isotherms associated with the subsurface patch (16 – 17 °C, Fig. 7c), possibly resulted from vertical mixing of the subsurface Chl *a* patch with warmer surface water. Here, the role of vertical mixing, including cross-isotherm mixing, in the surface appearance Chl *a* patch is investigated by examining the temporal evolution of the T-z and Chl *a*-T relationships from 1200 to 1500 h, within the 750 m-wide region between H = 5 to 12 m. This region bounds the Chl *a* patch (Fig. 4), includes the estimated time and location of sIW breaking (white star in Fig 5e), and excludes the warm shallow water (x < 200 m, H < 5 m, Fig. 4). To minimize the effects of cross-shore advection, CTD+Chl *a* cast-derived Chl *a* and T for each nearshore survey on 12 Oct were cross-shore-averaged (denoted $\langle \text{Chl } a(z) \rangle$ and $\langle T(z) \rangle$), into 1 m-thick vertical bins.

The depth-average of $\langle \text{Chl } a\ (z) \rangle$ remained roughly constant (within 15%) between 1200 and 1500 h, consistent with small depth-integrated cross-shore Chl *a* fluxes, and small net phytoplankton growth and mortality (not shown). The depth-averaged $\langle T(z) \rangle$ warmed slightly, from 16.9 to 17.1 °C, perhaps from solar heating. For each survey $\langle T(z) \rangle$ were approximately linear with depth (not shown). The vertical temperature gradient $d\langle T(z) \rangle/dz$ decreased monotonically, and the corresponding buoyancy frequency decreased from 0.018 s^{-1} at 1200 h to 0.016 s^{-1} at 1500 h, suggesting that vertical spreading of $T(z)$, dominated the stratifying effects of solar warming over the afternoon.

In addition to a reduction in N (implying vertical mixing), cross-isotherm Chl $a(z)$ mixing may also have occurred. For example, cross-isotherm Chl *a* spreading (and/or surface solar heating) may explain the appearance of the surface Chl *a* patch on the 17.5 °C isotherm at 1330 h (Fig. 4e,g,i), since Chl *a* was not present on this isotherm at 1200 h

(Fig. 4a). Subsurface cross-isotherm Chl *a* spreading was evident in the evolution of the cross-shore-averaged $\langle \text{Chl } a(z) \rangle$-$\langle \text{T}(z) \rangle$ relationship (Fig. 10). For all surveys, $\langle \text{Chl } a(z) \rangle$ was maximum near $T = 16.9$ °C. At 1200 h, $\langle \text{Chl } a(z) \rangle$ was concentrated over a narrow range of $T(z)$, and throughout the afternoon, $\langle \text{Chl } a(z) \rangle$ spread over a larger range of $T(z)$ (e.g., compare the dashed gray with the solid black curve in Fig. 10). Although the CTD+Chl *a* surveys exclude the top 1 m of data, the increased $\langle \text{Chl } a(z) \rangle$ at $\langle T(z) \rangle > 17.3$ °C after 1200 h, was in qualitative agreement with the surface manifestation of the patch (e.g., Fig. 4e-j).

Disappearance of Chl a in very shallow water

During the jetski-CTD observation period, the high Chl *a* surface patch did not enter the surfzone ($0 < x < 150$ m) where the near-surface water in the surfzone warmed relative to near-surface offshore waters (see Fig. 4). Between 1000 and 1200h, near-surface T was uniform at roughly 17 °C from within the surfzone to seaward of M13 (Fig. 11a). Coincident with the M13 subsurface Chl *a* peak (Fig. 3d), M4 Chl *a* (at 0.5 m above the seafloor) was elevated (between 5-10 $\mu g L^{-1}$), with the peak M4 Chl *a* only ~ 25% of that at M13 (Fig. 8), and varied on 1 h time-scales (solid black line, Fig. 11b). The M4 dinoflagellate (mainly *L. polyedrum*) cell concentrations also reached a maximum of 7.3×10^4 cellsL^{-1} near 1130 h (solid black line, Fig. 11c), while diatom abundance remained low $O(10^3)$ cells L^{-1} (dashed black line, Fig. 11c). The bottle sample collection rate was not rapid enough to resolve sub-hourly fluctuations. However, the qualitative agreement between dinoflagellate cell concentration and Chl *a* indicates that the M4 Chl *a* variation was due to variation in total dinoflagellates. Within the surfzone, Chl *a* was lower at about 3-4 $\mu g L^{-1}$ (Fig. 11b), consistent with the jetski-observed Chl *a*

values at 1200 h (Fig. 4a). In the surfzone, dinoflagellate (solid gray lines) and diatom (dashed gray lines) concentrations were low, usually < 10^4 cells L^{-1}, and relatively constant throughout the sample period (Fig. 11c).

At 1130 h, the M4 Chl *a* began dropping and by 1230 h reached the level at M1.5 (3 μgL^{-1}). M1.5 and M4 Chl *a* remained constant throughout the afternoon as *T* at both locations rose (Fig. 11). During mid-day, the near-surface M13 *T* also increased slightly (thin curve in Fig. 11a). By 1500 h, a cross-shore temperature gradient (with ΔT ~ 0.8 C) had developed with warmest water in the surfzone and cooler water offshore, consistent with surface *T* maps (Fig. 4j). The strong afternoon *T* gradient, and morning gradients in Chl *a*, total cells and community composition were maintained over only 80 m in the cross-shore.

Discussion

A dense patch containing 3X the mean concentration of the red-tide layer was observed at M13 (1100 h, Fig 8). The patch appears to have developed though local intensification through the interaction of depth-keeping swimming, with a shoreward-propagating internal wave trough. The supertidal internal wave arrival in shallow water (H < 12 m) coincided with vertical spreading of the Chl *a* patch, creating an alongshore Chl *a* band visible at the surface. Mechanisms underlying these processes are discussed.

Formation of the dense subsurface Chl a patch within a shoreward-propagating wave trough

A supertidal internal wave of depression (sIW) propagated onshore with a phase speed consistent with linear theory. The sIW propagated coherently past the mooring array (Fig 5), maintaining shape as it moved into shallower waters. The wave passage at M13 coincided with a concentrated patch of Chl *a* above the sIW trough and within the subsurface Chl *a* maximum layer. The patch may have formed through the combined effects of localized phytoplankton depth-keeping swimming and the IW-induced convergent flow (e.g. Lennert-Cody and Franks,1999). Though propagating nonlinear internal waves may transport particles in the direction of propagation above the wave trough (e.g. Lamb, 1997), the sIW phase velocity (between 0.015 to 0.012 ms^{-1}) was significantly larger than the mean Eulerian velocity within the wave trough at each mooring (between 0.07 to 0.03 ms^{-1} at M24 to M13 respectively). The Chl *a* patch was likely formed by local intensfication of the subsurface Chl *a* layer, with limited advection by relatively weak currents, as opposed to being advected from offshore within the wave trough. The high-concentration Chl *a* patch was estimated to be 200 m wide across shore. This is consistent with the cross-shore width of the surface Chl *a* patch (Fig. 4).

The relationship between the vertically averaged Chl *a* and depth of the 17 °C isotherm Dz (Fig. 8a) is consistent with theoretical predictions and previous observations (Lennert-Cody and Franks 1999, 2002): Chl *a* was enhanced in wave troughs where isotherms are strained. The amount of Chl *a* enhancement depends on the phytoplankton swimming proficiency relative to rate of the vertical movement of the isotherms. Typical instantaneous swimming speeds of *L. polyedrum* in the laboratory range between 100 and

400 mms^{-1} (Lewis and Hallet, 1997; Buskey, 1997; Mayali et al. 2008). Vertical velocities (*w*) estimated from vertical displacements of the 17.0 °C isotherm ranged between about 300-1500 mms^{-1} (e.g., 2-9 cm min^{-1}, see bold isotherm displacements between 1000 and 1500 h, Fig. 5d). The range in *w* partially overlaps the range of *L. polyedrum* swimming speeds, suggesting that the dinoflagellates could have partially or completely countered the sIW-generated vertical velocities.

Local Chl *a* enhancement above isotherm troughs indicates that Chl *a* is not a passive tracer in this region of large amplitude, shoreward-propagating, internal waves. Swimming may contribute significantly to deviations of the Chl *a* concentration from predictions of a passive tracer, but quantification requires more detailed understanding of both *L. polyedrum* swimming behavior, and of potential Lagrangian transport in nonlinear internal waves.

sIW breaking in shallow water

The sIW trough was not evident at M8 (H = 8 m, white star, Fig. 5e), possibly due to IW breaking (e.g., Cacchione and Wunsch, 1974). At M13 (H = 13 m), the sIW amplitude a_o was ~ 5 m, based on the vertical displacement (crest to trough) of the 17 °C isotherm (thick black contour, Fig. 5d). The group velocity of a shoreward-propagating internal wave decreases, and a_o increases, to conserve wave energy, until the wave breaks (e.g., Gill, 1982). For an idealized 2-layer system, breaking occurs when the undisturbed lower layer thickness D_{low} is less than D_{bp} (Helfrich, 1992) defined as

$$D_{bp} = \frac{a_o}{(1.6\frac{\lambda}{L} + 0.6)}, \qquad (2)$$

where λ is the wavelength and L is the distance to the shelf break; L = 8000 m at Huntington Beach, where H = 60 m depth. The ratio λ/L is small for supertidal IWs, and D_{bp} depends only weakly on λ. Using the observed C_p = 0.10 ms^{-1} and λ ~ 500 m) (given a wave period ~ 2 hrs) an idealized, sIW with a_o = 5 m, would begin breaking when D_{low} < D_{bp} ~ 7 m.

Taking the lower layer thickness D_{low} as the elevation of the 17.0 °C isotherm above the seafloor, D_{low} was 11 m before, and 8 m after, the trough passed M13 (Fig. 5d) and the sIW was not breaking according to (2). At M8 (H = 7.8 m), D_{low} was always less than D_{bp} (Fig. 5d,e) indicating that wave breaking has occurred according to (2). Helfrich's criteria (2), and the observed obscuring of the sIW trough, indicates that IW breaking occurred between M13 and M8. A projection of the linear relationship between C_p and H from (1) (Fig. 6b), predicts that the sIW likely began breaking near 1230 h (white star in Fig 5e).

Vertical mixing of Chl a

On 12 Oct, the peak horizontally-integrated nearshore Chl *a* decreased over time and Chl *a* was spread over a broadening range of isotherms (Fig. 10). The shoreward-propagating IW breaking was anticipated in H ~ 8 m, and may have mixed the water column vigorously enough for the subsurface bloom to reach the surface, where it was observed visually (Fig. 1) and with the jetski maps (Fig. 4c,e) as a 200 m-wide, surface patch onshore of M13. The vertical spreading of the subsurface $\langle$Chl $a(z)\rangle$ layer, which includes cross-isotherm mixing, is quantified. The $\langle$Chl $a(z)\rangle$ center of mass ($\langle z\rangle_{Chla}$) (e.g., Csanady, 1973),

$$\langle z\rangle_{Chla} = \frac{\int_{-H}^{0} z\langle Chla(z)\rangle dz}{\int_{-H}^{0} \langle Chla(z)\rangle dz}, \quad (3)$$

deepened linearly from -7.1 m to -7.8 m (Fig. 12a) over 3 hrs at a rate of 60 μms^{-1}. The deepening of the layer peak is qualitatively evident in the CTD+ Chl *a* sections (Fig. 4a,c,e,g,i). The phytoplankton layer squared half-width (σ^2_{Chla})(e.g., Csanady, 1973),

$$\sigma^2_{Chla} = \frac{\int_{-H}^{0} (z - \langle z\rangle_{Chla})^2 \langle Chla(z)\rangle dz}{\int_{-H}^{0} \langle Chla(z)\rangle dz}, \quad (4)$$

increased roughly linearly with time until slowing around 1500 h (solid line, Fig. 12b), as anticipated with breaking sIW turbulence. The layer width (2σ) varied between 4.2 m at 1200 h and 4.7 m at 1415 h, consistent with the qualitative Chl *a* vertical spreading seen in the CTD+Chl *a* sections (Fig. 4a,c,e,g,i). The slowing of the Chl *a* vertical spreading by 1500 h may be attributed to subsiding of the breaking sIW-generated mixing. The vertical diffusivity κ_{zz} and squared layer width σ^2 are related (e.g., Csanady, 1973),

$$\kappa_{zz} = \frac{1}{2}\frac{\partial \sigma^2_{Chla}}{\partial t} . \quad (5)$$

The best-fit linear slope of σ^2_{Chla} between 1200 and 1415 h (dashed line, Fig. 12b) yields κ_{zz} = 0.5 x 10^{-4} m^{2}s^{-1}, close to the range for diffusion of surface-layer (nitrate and temperature) of 0.6 x 10^{-4} to 3 x 10^{-4} m^{2}s^{-1} previously estimated on the Southern California shelf (e.g., Eppley et al. 1979; Dillon and Caldwell, 1980).

Phytoplankton swimming behavior is implicated in IW trough Chl *a* intensification at M13 (Fig. 9a). The 60 μms^{-1} downward velocity of the Chl *a* patch center of mass $\langle z\rangle_{Chla}$ between 1200 and 1415 h was small compared with typical *L*.

polyedrum swimming/sinking speeds (100 – 400 μms^{-1}), and swimming or advection could have caused the downward movement of $\langle z \rangle_{Chla}$ between 1200 and 1500 h. The potential Chl *a* vertical spreading rate owing to random phytoplankton swimming (akin to a random walk) can be scaled by $\frac{1}{2} \cdot \tau \cdot \hat{u}_s^2$ where $\hat{u}_s$ is a typical swimming speed, and τ the decorrelation time of swimming direction. Assuming $\hat{u}_s \sim 200$ μms^{-1}, $\tau = 40$ min is required to reproduce the observed κ_{zz}. This τ is implausible large, and would induce ballistic dispersion (ie. $\sigma^2_{Chla} \sim t^2$, Csanady, 1973), instead of the observed linear (Brownian) relationship (Fig. 12b). The vertical diffusion of the Chl *a* layer is not due to random phytoplankton swimming, and was likely induced by breaking internal wave turbulence. The expected sIW arrival time (~1230 h) based on (1), and the anticipated breaking of the IW onshore of M13 (based on (2), together with the evidence for vertical mixing of *T* and Chl *a*, suggest that sIW breaking drove the appearance of the surface alongshore Chl *a* band.

A warm-water barrier to the Chl a patch in the surfzone

The surface Chl *a* patch did not enter the surfzone. A strong gradient in *T*, Chl *a* and phytoplankton was observed over 80 m spanning the surfzone (Fig. 11). The warm > 18 °C surfzone water present at M1.5 and M4 after 1300 h likely originated from the Talbert Marsh, located 1 km South (+y) of the fixed instrument array (see Fig. 2), creating a barrier to Chl *a* entry into the surfzone from offshore. Before 1200 h, the flood tide (Fig. 7a) raised the marsh water level. Over the morning and early afternoon, the water within the shallow marsh ($H \sim 2$ m) was solar heated relative to near-surface temperatures at M13. Using the marsh area (10^5 m^3, Grant et al. 2001), tidal prism (2.35 x 10^5 m^3, Jeong et al. 2008) and the solar insolation, the marsh water would be heated

about 0.8 ^{o}C. With the ebb tide at 1200 h, the warmed marsh water began draining into the surfzone. The 0.15 ms^{-1} northward surfzone alongshore current (see Fig. 4), driven by obliquely incident breaking surface gravity waves (e.g., Longuet-Higgins, 1970), transported this water to the study region. The predicted increase of ~0.8 °C at M1.5 and M4 is roughly consistent with the near-surface *T* gradient that developed between the surfzone M1.5 and M13. The *T* increase coincided with the reduction of Chl *a* at M4 (Fig. 11) and suppressed exchange between the surfzone and the water seaward. If the warm water had not been present, the intense Chl *a* patch may have entered the surfzone.

Summary and synthesis

Observations and mechanisms underlying the sudden surface appearance of a nearshore red tide have been described. The kilometer-long shore-parallel surface Chl *a* band (maximum Chl *a* = 7 μgL^{-1}) persisted for approximately 3 hrs at *H* = 6-8 m with a cross-shore width of 200 m. A subsurface red tide layer (dominated by *Lingulodinium polyedrum*) developed in the nearshore over 4-7 days prior to the appearance of the patch at the surface. At the M13, an elevated Chl *a* patch was observed in the trough of a supertidal internal wave (sIW) that propagated coherently across the mooring array (Fig. 13a). The elevated Chl *a* in the sIW trough is consistent with phytoplankton swimming and IW-induced convergent flow intensifying Chl *a*. Based on the estimated phase speed, the sIW arrived in shallow water (< 12 m) around 1230 h, where wave breaking was anticpated, generating turbulence that led to vertical mixing and the appearance of the Chl *a* patch at the surface (Fig. 13b). The wave arrival time (1230 h), the approximate patch width (200 m), and depth of anticipated wave breaking (H ~ 8 m) are consistent with the appearance and dimensions of the surface Chl *a* band (Fig. 4).

Between 1400 and 1700 h, the lower portion of the vertically spread Chl *a* patch appears to have been advected offshore past M13 with the baroclinic cross-shore currents (Fig. 8). The surface Chl *a* patch persisted at a warmer isotherm (> 17.5 ^{o}C) than originally associated with the Chl *a* patch (Fig. 13c), consistent with cross-shore mixing. The surface Chl *a* patch was transported offshore past M13 after 1600 h by the offshore-directed surface currents once the baroclinic internal tide had reversed (Fig. 13d).

The drivers of Chl *a* distributions in the nearshore are complex. The interaction between motile phytoplankton and tidal currents, propagating internal waves, breaking internal waves, and surface wave-driven surfzone currents can create phytoplankton patchiness and dramatic spatial and temporal changes in community structure over 10's of meters and 10's of minutes. These mechanisms that concentrate, advect, and mix nearshore phytoplankton, changing exposure durations and intensity, may have large consequences for the ecology of the nearshore region.

Web Appendix: Corrections for Non-Photochemical Quenching (NPQ)

Chl *a* concentration is linearly related to Chl *a* fluorescence under most oceanic conditions (Lorenzen, 1966). However, *in situ* Chl *a* fluorescence measurements can be biased low due to a phytoplanktonic physiological adaptation called nonphotochemical quenching (NPQ: Kiefer 1973, Falkowski and Raven 1997, Muller et al. 2001). NPQ protects cells from high light conditions near the surface. To prevent cell damage from light absorption beyond the saturated capacity for photosynthesis, a fraction of the excess light energy is converted by the cell to heat, rather than fluorescence. The result is reduced fluorescence capacity per cell, leading to underestimation of fluorescence-derived near-surface daylight Chl *a* concentration.

Here, NPQ correction of fluorescence-derived Chl *a* was based upon the cell's estimated local light environment (following Hodges, 2006). A similar approach presented in Todd et al. (2009) with a correction based on local irradiance, produced a nearly identical result (maximum 6.9% difference) to the Chl *a* correction presented below. The 'corrected' Chl *a* (z,t) (in the absence of NPQ) is a function of the fluorescence measured Chl *a*, Chl a_m(z,t), and a quenching function *Q(z,t)*, i.e.,

$$Chla(z,t) = \frac{Chla_m(z,t)}{Q(z,t)} \ , \qquad \text{(A1)}$$

where *Q(z,t)* is a function of local irradiance $\phi(z,t)$. Hodges (2006) suggests a functional form for *Q(z,t)*,

$$Q(z,t) = \frac{k}{k + \phi^*(z,t)}, \qquad \text{(A2)}$$

where *k* is a constant, and $\phi^*(z,t)$ is the normalized local irradiance. The downward surface ($z = 0$) irradiance $\phi_o(t)$ was measured for 24 hrs near the field site on 16 Oct 2006, 4 days after the red tide observations (12 Oct). Both 12 Oct and 16 Oct were sunny,

cloudless days, thus 16 Oct $\phi_o(t)$ was assumed representative of surface irradiance conditions during similar days at HB06. Surface irradiance was normalized by the maximum surface irradiance, i.e., $\phi_o^*(t) = \phi_o(t)/\phi_{omax}$. Irradiance was assumed to decrease exponentially with depth according to $\phi(z,t) = \phi_o(t)e^{-z/\gamma}$ where γ is the unknown decay scale estimated from the vertical length scale of the covariation of Chl $a_m(z,t)$ with $\phi_o^*(t)$. The red tide time (5 Oct through 16 Oct) period was not used due to the intense subsurface Chl *a* layer with large vertical excursions over a 24 hr period (see Fig. 7c) that would complicate the estimation of γ. Instead, the time period from 20-25 Sept 2006, when M13 Chl $a_m(z,t)$ was low (1 - 4 μgL^{-1}) with no subsurface maxima, was used for the covariation analysis. Chl $a_m(z,t)$ covaried with $\phi_o^*(t)$ at the surface ($r^2 = 0.50$, $p < 0.01$). The correlation diminished with depth over an e-folding scale $\gamma = 9.7$ m. This γ is comparable to prior estimates ($\gamma \sim 5$ - 11 m) from coastal waters in the Southern California Bight (e.g., Holmes, 1970, Conversi and McGowan, 1994).

In (A2), the optimal $k = 1.6$ was chosen to minimize the correlation between Chl $a(z,t)$ and $Q(z,t)$, resulting in $Q(z,t)$ ranging between 0.615 and 1. Under maximum irradiance [i.e., ϕ_o^*(1200 h) = 1], near-surface Chl *a* was enhanced by 56% relative to Chl a_m, similar to Hodges (2006) finding that the maximum near-surface correction was roughly 100% Chl a_m. The NPQ correction derived in (A1) and (A2) was applied to all *in situ* Chl a_m measurements (CTD+Chl *a*, M13, M1.5, M4, see Fig. 1) presented here. Although the NPQ correction modified Chl *a* concentrations as much as 2X near the surface, the patterns described here were also present in uncorrected data. For example, along the 17 ^oC isotherm the maximum NPQ correction imposed a 9% change from the raw measurement; insufficient to explain the 3X Chl *a* increase observed in the sIW trough.

References

Alonso-Rodrígueza, R., and F. Páez-Osuna (2003) Nutrients, phytoplankton and harmful algal blooms in shrimp ponds: a review with special reference to the situation in the Gulf of California. Aquaculture, 219, 317-336.

Anderson, D. M. (1997) Turning back the harmful red tide. Nature, 388, 513–514.

Backer, L. C., L. E. Fleming, A. Rowan, Y. Chen, J. Bensone, R. H. Pierce, J. Zaias, J. Bean, G. D. Bossarth, D. Johnson, R. Quimbo, and D. G. Baden (2003) Recreational exposure to aerosolized brevetoxins during Florida red tide events. Harmful Algae, 2(1), 19-28.

Boehm, A. B., S. B. Grant, J. H. Kim, S. L. Mowbray, C. D. Mcgee, C. D. Clark, D. M. Foley, and D. E. Wellman (2002) Decadal and shorter period variability of surf zone water at Huntington Beach, California. Environmental Science and Technology, 36(18), 3885–3892.

Boehm A. B., B. F. Sanders, and C. D. Winant (2002), Cross-shelf transport at Huntington Beach. Implications for the fate of sewage discharged through an offshore Ocean outfall, Environmental Science and Technology, 36(9), 1899-1906.

Bretherton, F. P., R. E. Davis, and C. B. Fandry (1976) A technique for objective analysis and design of Oceanographic experiments Applied to MODE-73. Deep Sea Research, 23, 559-582.

Bricelj, V. M., J. H. Lee, A. D. Cembella, and D. M. Anderson (1990) Uptake kinetics of paralytic shellfish toxins from the dinoflagellate *Alexandrium fundyense* in the mussel *Mytilus edulis.* Marine Ecology Progress Series, 63, 177-188.

Buskey, E. J. (1997) Behavioral components of feeding selectivity of the heterotrophic dinoflagellate *Protoperidinium pellucidum.* Marine Ecology Progress Series, 153, 77-89.

Cacchione, D., and C. Wunsch (1974), Experimental study of internal waves over a slope, Journal of Fluid Mechanics, 66, 223-239.

Campbell, E. E., and G. C. Bate (1988) The influence of current direction on longshore distribution of surf phytoplankton. Botanica Marina, 31(3), 257–262.

Clancy, M., and C. E. Epifanio (1989), Distribution of crab larvae in relation to tidal fronts in Delaware Bay, USA, Marine Ecology Progress Series, 57, 77-82.

Clark, D. B., F. Feddersen, M. M. Omand, and R. T. Guza (2009) Measuring fluorescent dye in the bubbly and sediment-laden surfzone. Water, Air & Soil Pollution, DOI: 10.1007/s11270-009-0030-z.

Cloern, J. E. and R. Dufford, (2005), Phytoplankton community ecology: Principles applied in San Francisco Bay, Marine Ecology Progress Series, 285, 11-28.

Conversi, A., and J. A. McGowan (1994) Natural versus human-caused variability of water clarity in the Southern California Bight, Limnology and Oceanography, 39(3), 632-648.

Cox, E. R. (1980), Phytoflagellates. Elsevier/North-Holland, New York.

Csanady, G. T. (1973), Turbulent Diffusion in the Environment, D. Reidel, New York.

Dillon, T. M., and D. R. Caldwell (1980) The Batchelor spectrum and dissipation in the upper ocean. Journal of Geophysical Research, 85, 1910–1916.

Eppley, R. W., E. H. Renger, and W. G. Harrison (1979) Nitrate and phytoplankton production in Southern California coastal waters. Limnology and Oceanography, 23 (3), 483–494.

Falkowski, P., and J. A. Raven (1997) Aquatic photosynthesis. Blackwell Science.
Franks, P.J.S., and D. M. Anderson (1992), Alongshore transport of a toxic phytoplankton bloom in a buoyancy current: *Alexandrium tamarense* in the Gulf of Maine. Marine Biology, 112(1), 153-164.

Franks, P. J. S. (1997), Spatial patterns in dense algal blooms, Limnology and Oceanography, 4, 1297-1305.

Gallager, S.M., H. Yamazaki, and C. S. Davis (2004) Contribution of fine-scale vertical structure and swimming behavior to formation of plankton layers on Georges Bank. Marine Ecology Progress Series, 267, 27-43.

Gill, A. E. (1982) Atmosphere-Ocean Dynamics. Academic Press, New York.

Grant, S. B., B. F. Sanders, A. B. Boehm, J. A. Redman, J. H. Kim, R. D. Mrse, A. K. Chu, M. Gouldin, C. D. McGee, N. A. Gardiner, B. H. Jones, J. Svejkovsky, G. V. Leipzig, and A. Brown (2001) Generation of enterococci bacteria in a coastal saltwater marsh and its impact on surf zone water quality. Environmental Science and Technology, 35(12), 2407-2416.

Helfrich, K. R., (1992), Internal Solitary wave breaking and run-up on a uniform slope, Journal of Fluid Mechanics, 242, 1333-154.

Hodges, B. A. (2006) On the Distribution of Oceanic Chlorophyll. Ph.D. thesis. Univ. of California, San Diego.

Holmes, R. W. (1970) The Secchi disk in turbid coastal waters. Limnology and Oceanography, 15(5), 688-694.

Jeong, Y., B. F. Sanders, K. McLaughlin, and S. B. Grant (2008) Treatment of Dry Weather Urban Runoff in Tidal Saltwater Marshes: A Longitudinal Study of the

Talbert Marsh in Southern California. Environmental Science and Technology, 42 (10), 3609-3614.

Johnson, D. R., A. Weidemann, and W. S. Pegau, (2001) Internal tidal bores and bottom nepheloid layers. Continental Shelf Research, 21, 1473-1484.

Keafer, B.A. (2005), Bloom development and transport of toxic *Alexandrium fundyense* populations within a coastal plume in the Gulf of Maine. Deep-Sea Research. Part II, Topical Studies in Oceanography, 52(19), 2674-2697.

Kiefer, D. A. (1973), Chlorophyll a fluorescence in marine centric diatoms: Responses of chloroplasts to light and nutrient stress, Marine Biology, 23(1), 1432-1793.

Kullenberg, G. E. (1978) Vertical processes and the vertical-horizontal coupling. In J. H. Steele [ed.], Spatial pattern in plankton communities. Plenium, 43–72.

Lamb, K. G. (1997) Particle transport by non-breaking, solitary internal waves. Journal of Geophysical Research, 102(C8), 18, 641–18, 660.

Leichter, J. L., G. Shellenbarger, S. J. Genovese, and S. R. Wing (1998), Breaking internal waves on a Florida (USA) coral reef: a plankton pump at work? Marine Ecology Progress Series, 166, 83-97.

Lennert-Cody, C. E., and P. J. S. Franks (1999) Plankton patchiness in high-frequency internal waves. Marine Ecology Progress Series, 186, 59–66.

Lennert-Cody, C. E., and P. J. S. Franks (2002) Fluorescence patches in high-frequency internal waves. Marine Ecology Progress Series, 235, 29-42.

Lerczak, J. A. (2000) Internal waves on the Southern California Coast. Phd dissertation, University of California, San Diego.

Lewis, J. and Hallett, R. (1997) *Lingulodinium polyedrum* (*Gonyaulax polyedra*) a blooming dinoflagellate. Oceanogr. Mar. Biol. Annu. Rev., 35, 97-161.

Longuet-Higgins, M. S. (1970) Longshore currents generated by obliquely Incident Sea Waves, 1. Journal of Geophysical Research, 75(33), 6778-6789.

Lorenzen, C. J., (1966), Determination of chlorophyll in seawater, Deep Sea Research, 13, 223–22.

Mayali, X., P. J. S. F. Franks, Y. Tanaka, and F. Azam (2008) Bacteria-induced motility reduction in *Lingulodinium polyedrum* (Dinophyceae). Journal of Phycology, 44, 923-928.

Muller, P., X. Li, and K. K. Niyogi (2001) Non-photochemical quenching. A response to excess light energy. Plant Physiology, 125, 1558–1566.

Noble, M. A., B. Jones, P. Hamilton, J. Xu, G. Robertson, L. Rosenfeld, and J. Largier (2009) Cross-shore transport into nearshore waters due to shoaling internal tides in San Pedro Bay, CA. Continental Shelf Research, doi:10.1016/j.csr. 2009.04.008.

Noble, M. A. and J. P. Xu (2003) Observations of large-amplitude cross-shore internal bores near the shelf break, Santa Monica Bay, CA. Marine Environmental Research, 56(1-2), 127-149.

Omand, M. M., F. Feddersen, D. B. Clark, P. J. S. Franks, J. L. Leichter, and R. T. Guza, (2009) Influence of bubbles and sand on chlorophyll-a fluorescence measurements in the surfzone. Limnology and Oceanography: Methods, 7, 354-362.

Pineda, J., (1999), Circulation and larval distribution in internal tidal bore warm fronts. Limnology and Oceanography, 44, 1400–1414.

Rainville, L., and R. Pinkel (2001), Wirewalker: An autonomous wave-powered vertical profiler, Journal of Atmospheric and Oceanic Technology, 18(6), 1048-1051.

Santoro, A. E., N. J. Nidzieko, G. L. van Dijken, K. R. Arrigo, and A. B. Boehm (2010), Contrasting spring and summer phytoplankton dynamics in the nearshore Southern California Bight, Limnology and Oceanography, 55(1), 264–278.

Smith, W. O., G. W. Heburn, R. T. Barber, and J. J. O'Brien, (1983), Regulation of phytoplankton communities by physical processes in upwelling ecosystems, Journal of Marine Ecosystems, 41(3), 539-556.

Sullivan J.M., and E. Swift (2003) Effects of small-scale turbulence on net growth rate and size of ten species of marine dinoflagellates. Journal of Phycology, 39, 83-94.

Talbot, M. M., G. C. and Bate (1986) Diel periodicities in cell characteristics of the surfzone diatom *Anaulus birostratus*: Their role in the dynamics of cell patches. Marine Ecology Progress Series, 32, 81–89.

Todd, R. E., D. L. Rudnick, and R. E. Davis (2009), Monitoring the greater San Pedro Bay region using autonomous underwater gliders during fall of 2006, J. Geophys. Res., 114, C06001, doi:10.1029/2008JC005086.

Utermohl, H. (1958) Zur vervollkommnung der quantitativen phytoplankton-methodik. Mitteilungen. Internationale Vereiningung fuer Theoretische und Angewandte Limnologie, 52(9), 1–38.

Weiters E. A., D. M. Kaplan, S. A. Navarrete, A. Sotomayer, J. Largier, K. J. Nielsen and F. Veliz (2003) Alongshore and temporal variability in chlorophyll*a* concentration in Chilean nearshore waters. Marine Ecology Progress Series, 249, 93-105.

Winant, C. D. (1974) Internal surges in coastal waters. Journal of Geophysical Research, 79, 4523-4526.

Winant, C. D., and J. R. Olsen (1976) The vertical structure of coastal currents. Deep Sea Research, 23, 925-936.

Tables

Table 1. Composition of phytoplanktonic genera on 12 Oct within the nearshore (H < 15 m depth) and offshore (H > 15 m) regions. Dinoflagellates are identified in bold type.

Genus	**% Nearshore**	**% Offshore**
Lingulodinium	**71.6**	**4.9**
Chaetoceros	6.4	34.8
Asterionella	6.3	32.9
Prorocentrum	**4.6**	**0.9**
Psuedo-nitzschia	4.3	7.1
Skeletonema	0.6	7.5
Other	6.1	11.9

Table 2. Separation distance (Δx), time lag maximizing r^2 (Δt) and correlation coefficient (r^2) of the IW depth contours (Fig. 9b) between neighboring moorings. All correlations are significant at the 99% level.

Location	***Δx* (m)**	***Δt* (h)**	r^2
M24 to M18	1643	2.9	0.75
M18 to M15	715	1.6	0.63
M15 to M13	549	1.3	0.79

Figures

Figure 1. Un-retouched photograph of a reddish alongshore-parallel band of red tide (arrow) approximately 500 m offshore, taken from the beach in early afternoon on 12 Oct The small breaking surface wave in the foreground is near the beach, and the 5 m long CTD+Chl *a* cast boat is offshore.

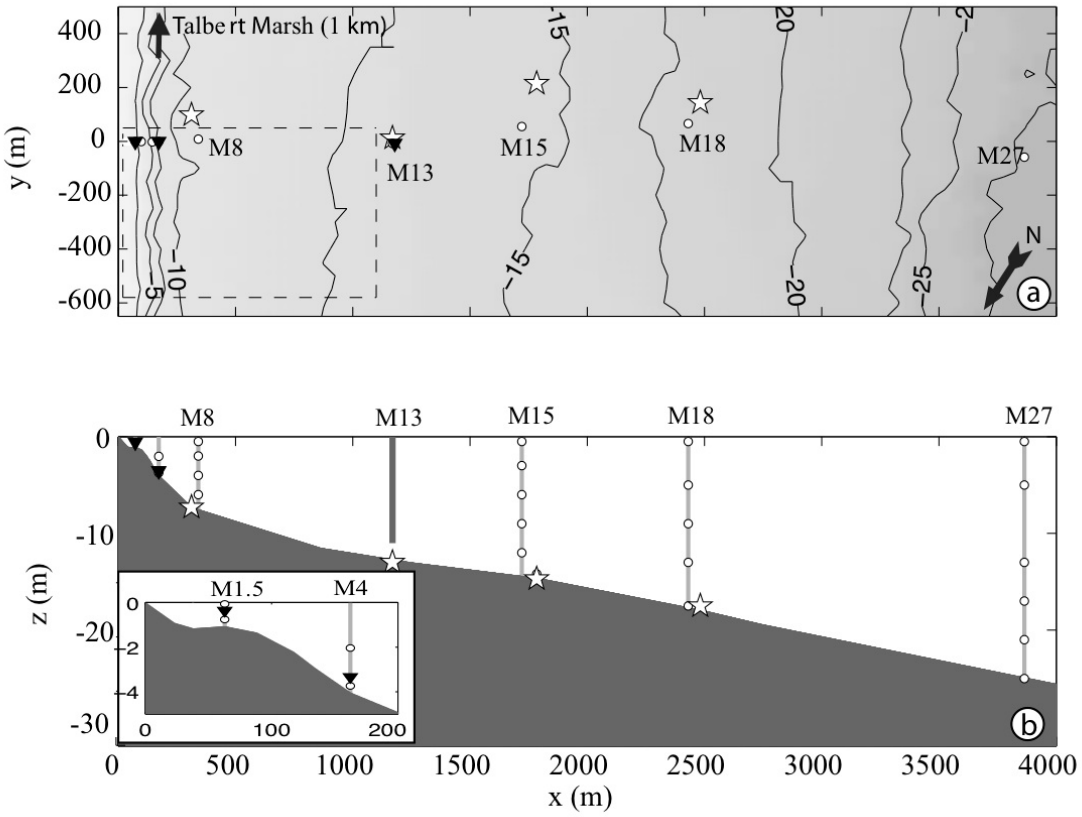

Figure 2. Schematic of HB06 instrumentation: (a) plan view of bathymetry contours versus the alongshore (*y*) and cross-shore (*x*) coordinates and (b) cross-shore transect of bathymetry (dark shading). The vertical coordinate is *z*, with *z* = 0 m at the tidally averaged surface and positive upward. Moored temperature strings were located at total depths *H* = 8, 15, 18 and 24 m (circles, M8 to M24). A vertically profiling CTD+Chl *a* wirewalker (M13) was located at *H* =13 m. Bottom-mounted ADCPs were located near moorings M8, M13, M15 and M18 (stars). Fixed frames within the surfzone (M1.5) at H = 1.5 m and seaward of the surfzone (M4) at H = 4 m measured Chl *a* (triangles), *T* (circles), wave height, and currents (see inset in (b)). A GPS-tracked jetski measured surface *T* and Chl *a* within the black dashed box in (a) and small boat (CTD+Chl *a*) completed transects during daylight hours from *H* = 5 to 60 m (~8 km offshore). The Talbert Marsh outlet is located ~1 km south of the instrument transect.

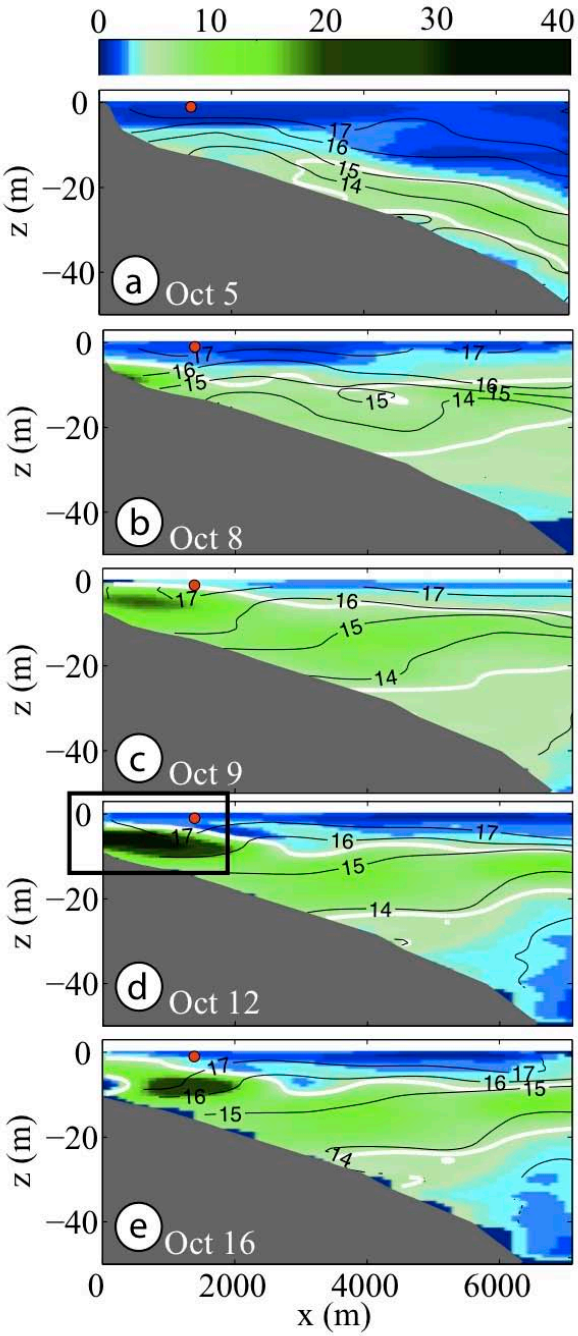

Figure 3. Cross-shore sections (*x*,*z*) of Chl *a* (μgL^{-1}, colors) and *T* (°C, black contours) conducted roughly between 0900 and 1130 h from 5 Oct to 16 Oct .The red circle is M13 surface location. The white line traces the 4 μgL^{-1} Chl *a* contour. The black box indicates the nearshore red tide focus area on 12 Oct.

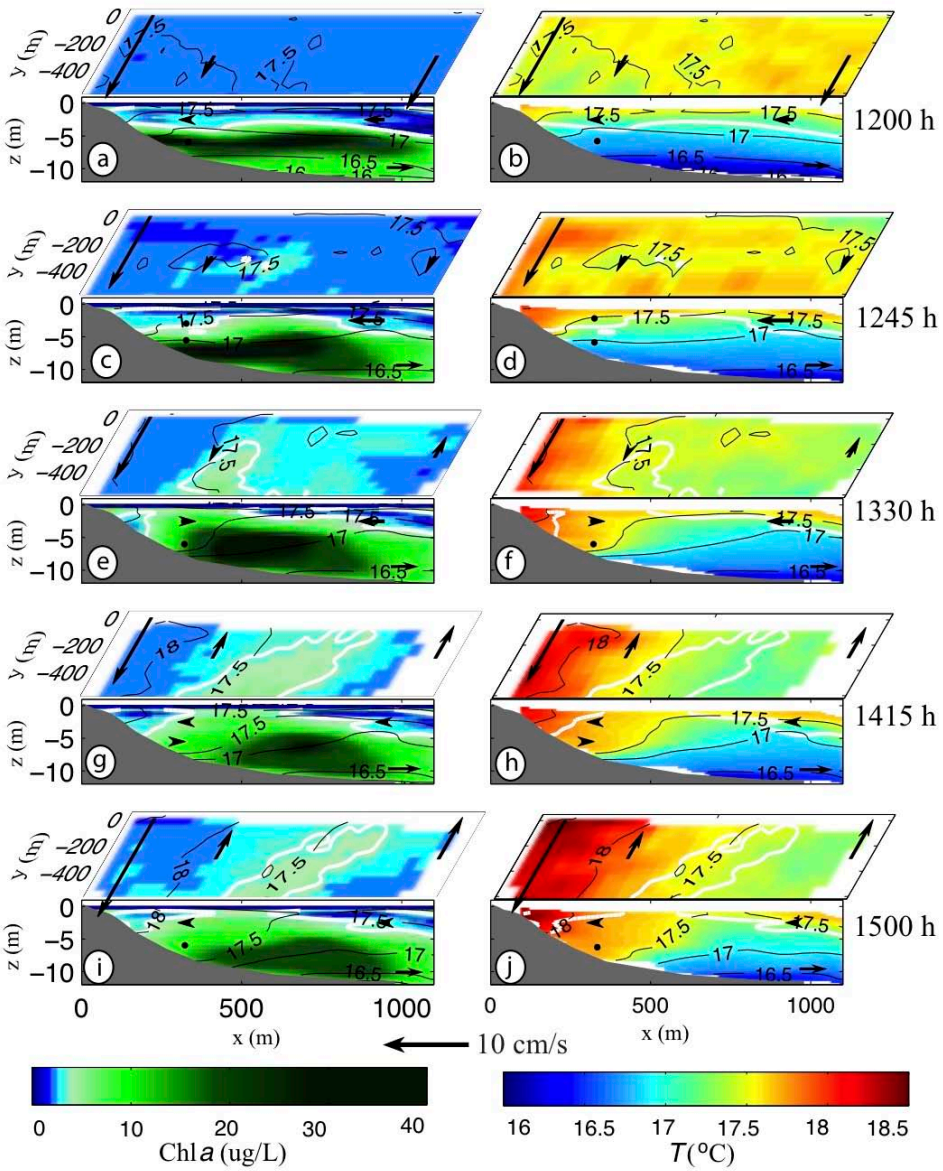

Figure 4. Sequential (top to bottom) maps of nearshore Chl *a* (left) and *T* (right) on 12 Oct from jetski-based horizontal (*x*,*y*) measurements and CTD+Chl *a* based cross-shore transect (*x*,*z*) measurements. Arrows represent the directions of the near-surface alongshore (at M1.5, M8 and M13) and near-surface (~2 m below mean sea level) and near-bottom (~ 2 m above the seafloor) cross-shore currents (at M8 and M13 only). The jetski required 30 min to complete the 8 cross-shore transects used for each map, and the centered-time (1200-1500 h) is shown to the right of each panel. Each CTD+Chl *a* transect consisted of 5 or 6 casts. Black lines are temperature contours. The white line traces the 4 μgL^{-1} Chl *a* contour.

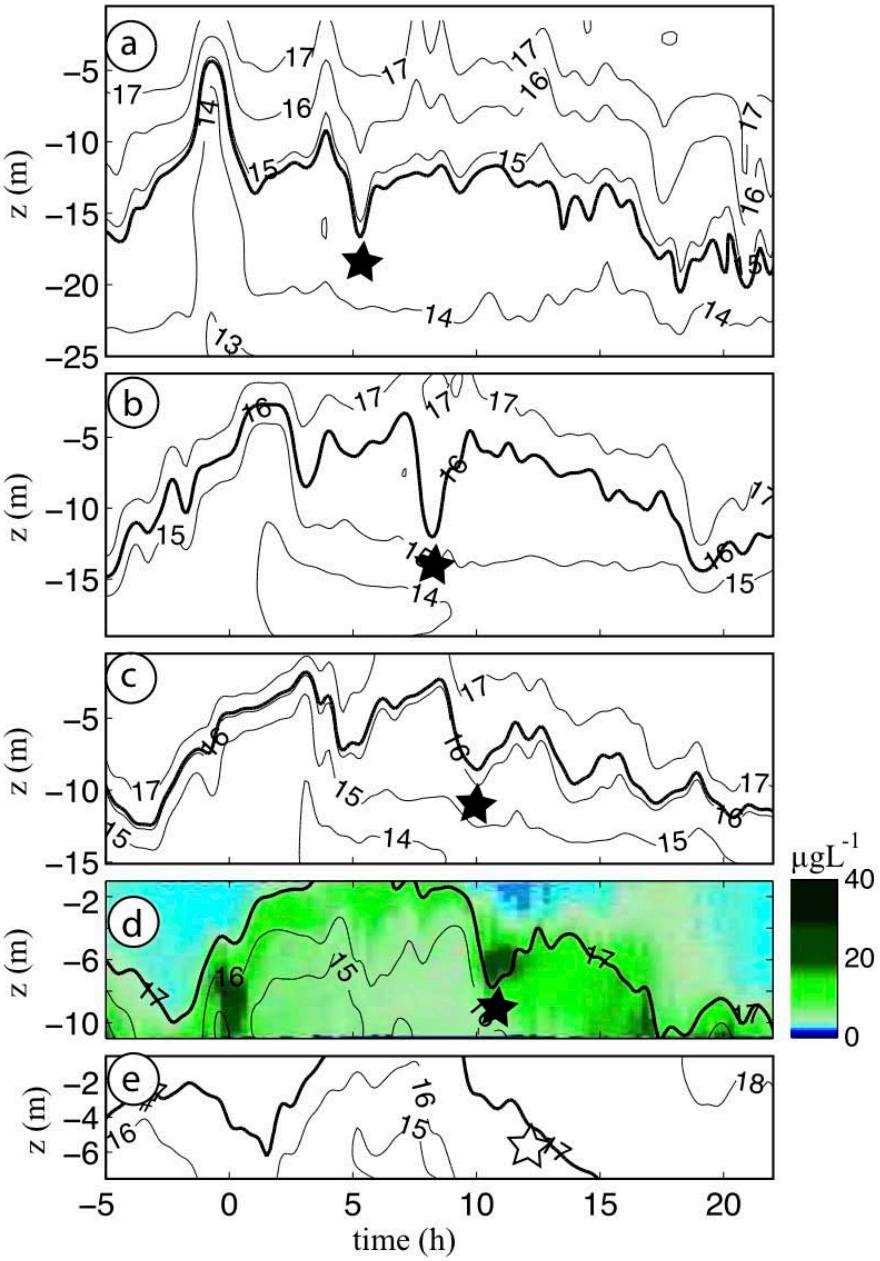

Figure 5. Contours of T (^{o}C) versus time and z at (a) M24, (b) M18, (c) M15, (d) M13, (e) M8. Black stars represent an internal wave trough (see bold contours) which can be seen to propagate onshore. The white star is the trough location at M8 predicted by linear theory. In (d) M13, Chl a (μgL^{-1}) is colored. Time zero corresponds to 0000 h 12 Oct.

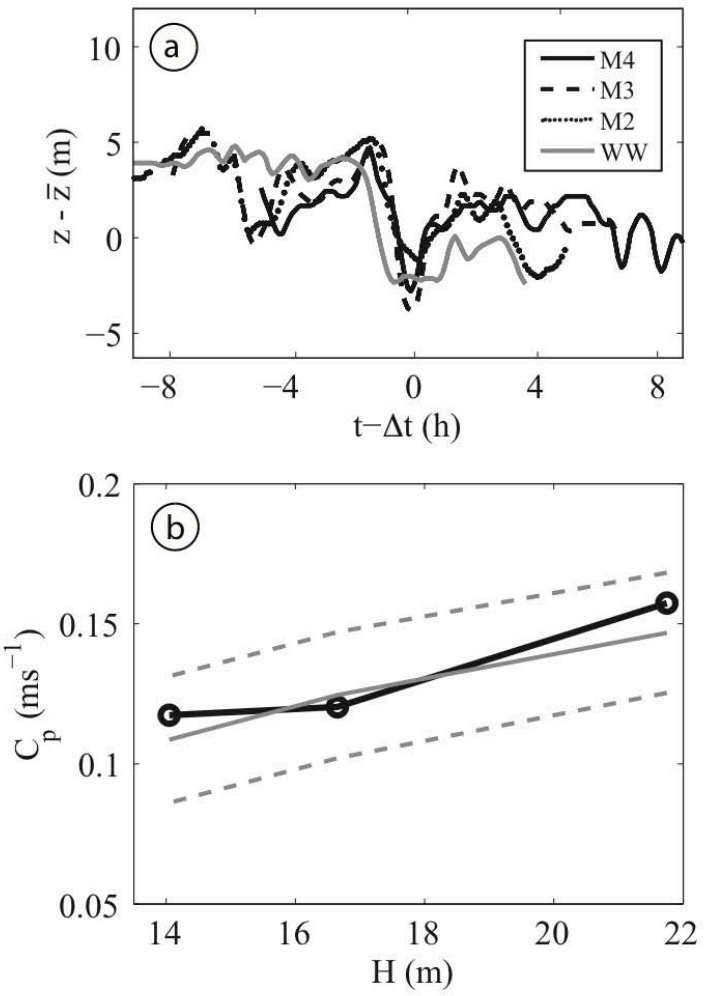

Figure 6. (a) Depth anomaly of mid water-column isotherms (bold contours in Fig. 5) versus lagged time (t-Δt) at M24, M18, M15, and M13 (see legend), with Δt for each mooring chosen to place the isotherm trough minimum at t=0. (b) Observed (solid black line) and theoretical phase velocity C_p (solid gray line, eq. 1) versus the water depth H. The observed $C_p = \Delta x/\Delta t$ was estimated midway between neighboring moorings, with Δx the mooring separation. The theoretical C_p is for a linear, mode-one IW with 2 h period, and using the depth-averaged buoyancy frequency N (solid gray) plus/minus standard deviation of N (dashed gray) between moorings.

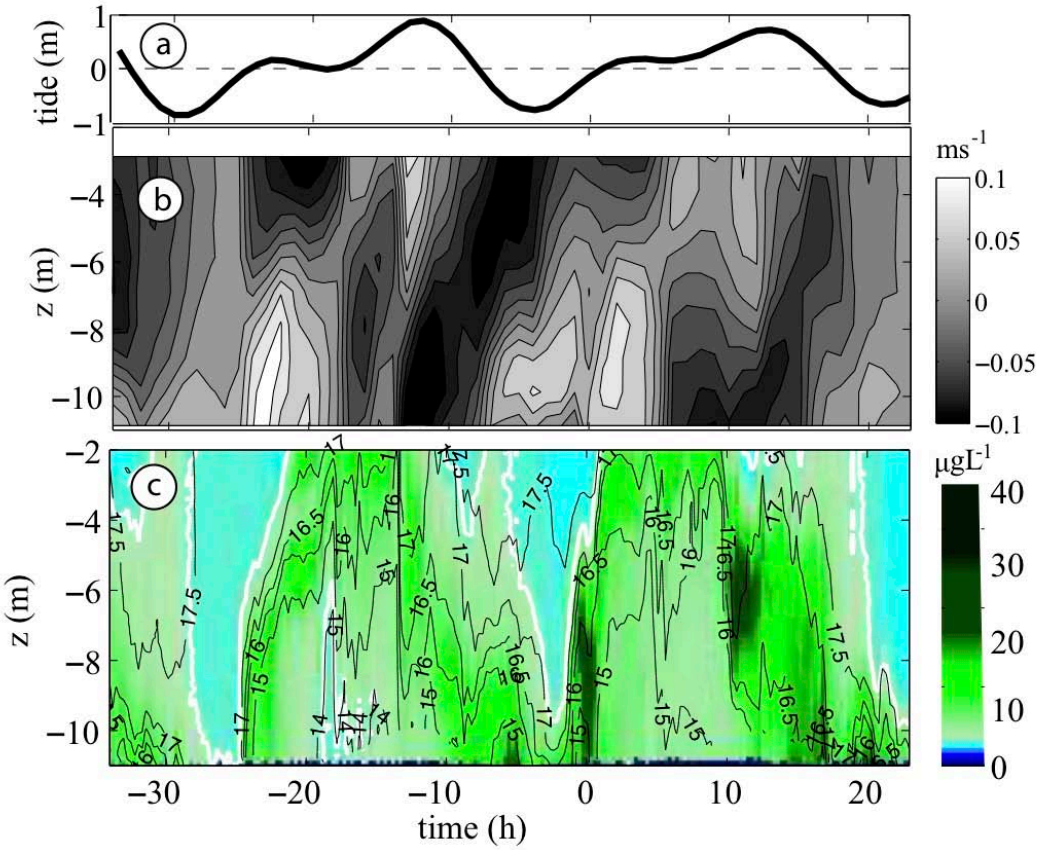

Figure 7. Time series (spanning 54 hrs) at M13 (H= 13m) of (a) tidal excursion from mean sea level, (b) vertical profiles of hourly averaged cross-shore currents *u* at M13 (positive = onshore) and (c) 15 min averaged vertical profiles of Chl *a* (µgL^{-1}, colors) and *T* ($^{\circ}$C, black contours) at M13. The white curves trace the 4 µgL^{-1} Chl *a* contour. Time zero is 0000 h 12 Oct.

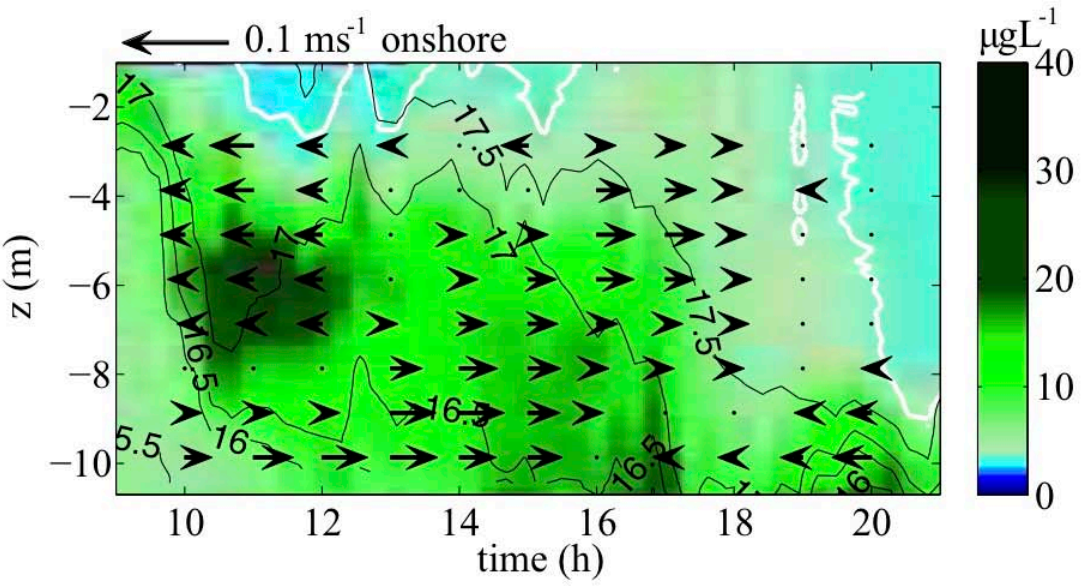

Figure 8. Time series (spanning 11 hrs of Fig. 7) of 15-min averaged vertical profiles of Chl *a* (µgL^{-1}, colors) and *T* ($^{\circ}$C, black contours) at M13 (*H* = 13 m). Time 10 hours corresponds to 1000 h on 12 Oct. The hourly averaged cross-shore currents (*u*) are represented by arrows for $|u| \geq 0.01$ ms^{-1} and by black dots where $|u| < 0.01$ ms^{-1}. The white line is the 4 µgL^{-1} contour.

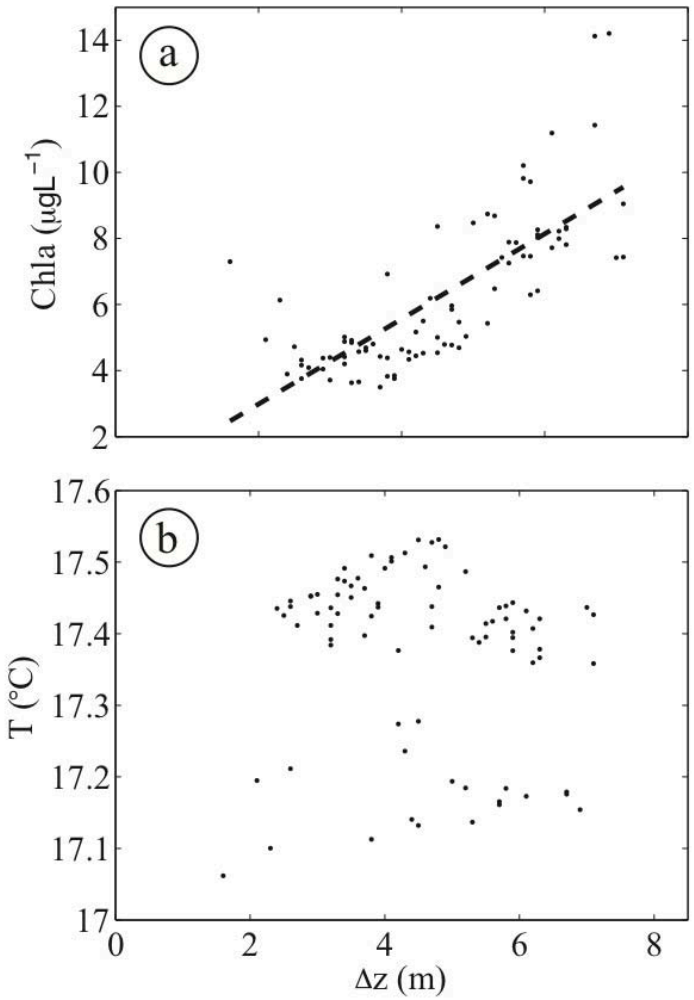

Figure 9. Vertically averaged (a) Chl *a* and (b) *T* above the 17.0 °C isotherm versus isotherm depth (Δz) at 4 min intervals between 0600 and 1700 h (number of data points, n = 165) on 12 Oct 2006. In (a), the best linear fit (dashed line) has slope 1.29 ± 0.03 μgL^{-1}m^{-1}, and $r^2 = 0.57$, $p < 0.01$. In (b) $r^2 = 0.013$, $p > 0.1$.

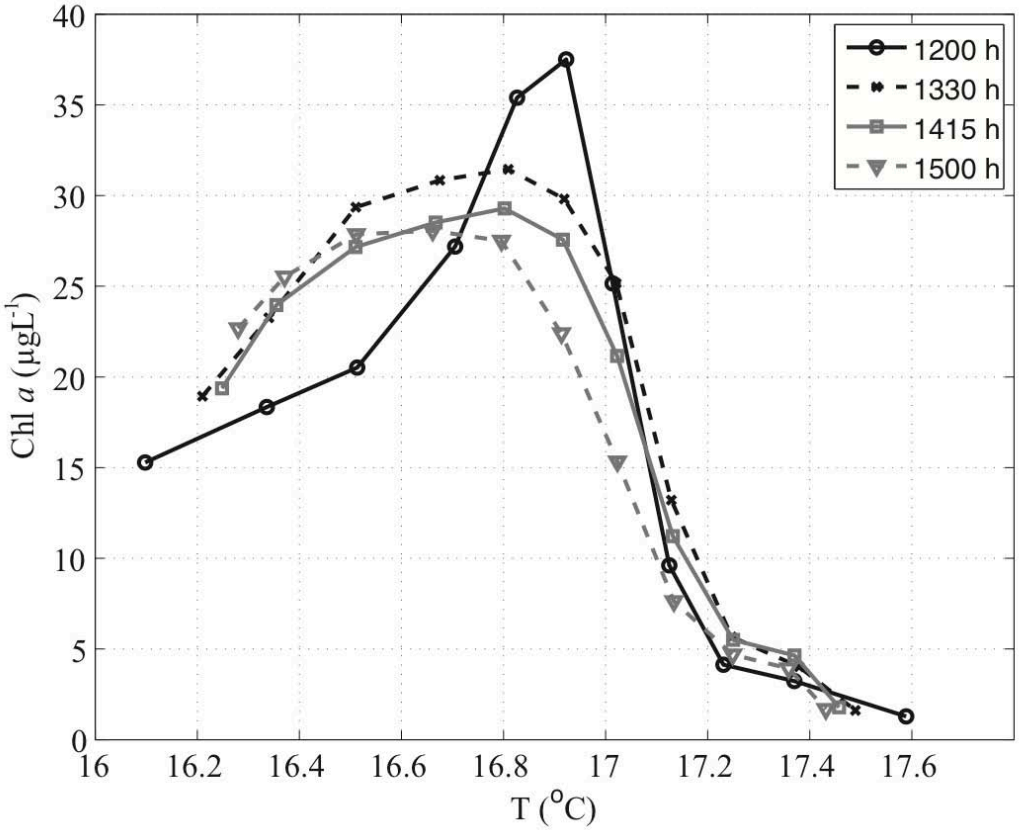

Figure 10. Chl *a* versus *T* (at 1200, 1330, 1415, and 1500 h) based upon the CTD+Chl *a* surveys (between *H* = 5 to 12 m depth, see Fig. 4) horizontally averaged along 1 m isobars.

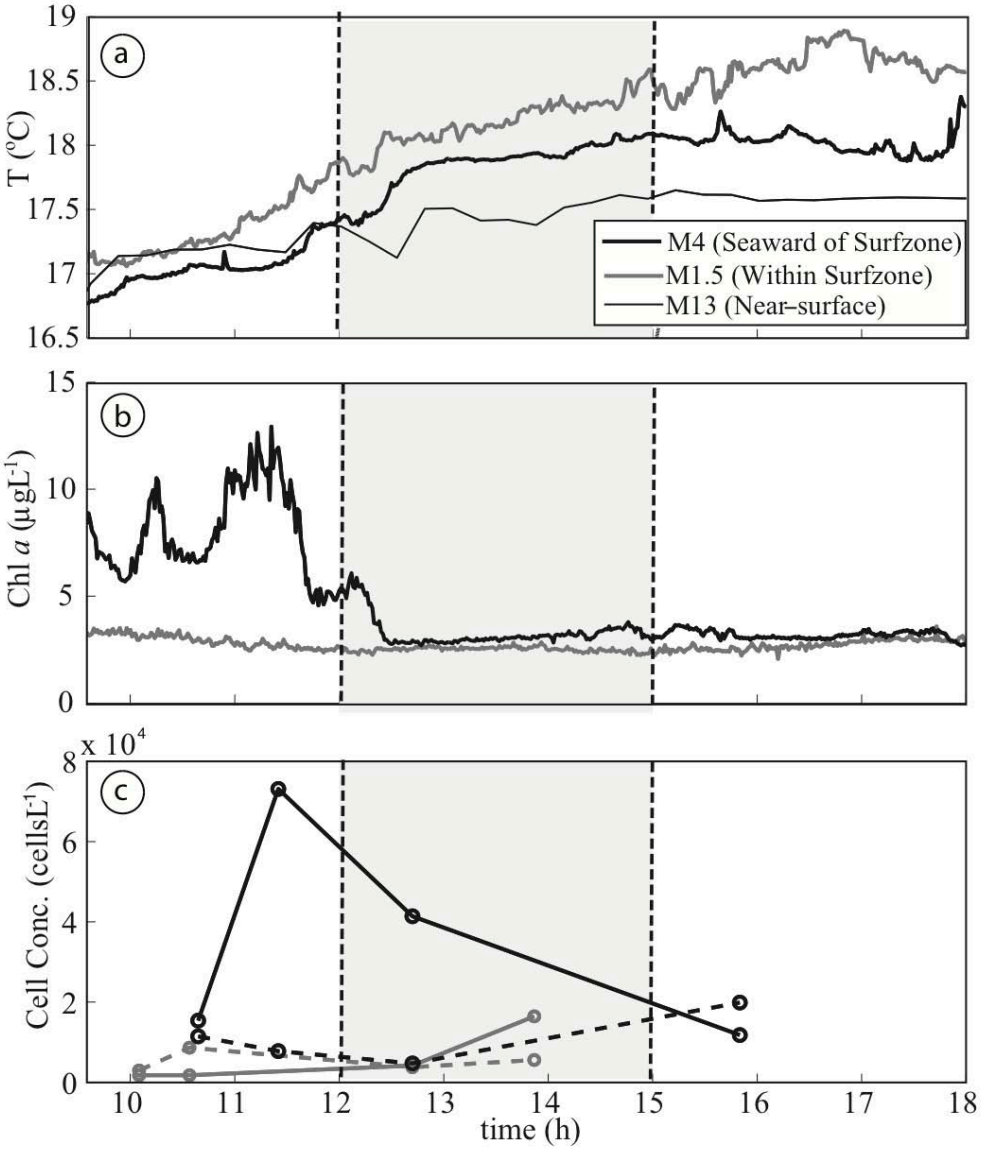

Figure 11. Time series from 0930 to 1800 h on 12 Oct of (a) *T* (1 min averages), (b) Chl *a* (1 min averages) and (c) dinoflagellate (solid) and diatom (dashed) concentrations from M4 (*H*= 4m) and M1.5 (*H* = 2 m), and in (a) 20 min average *T*, 2 m below the mean sea surface at M13 (H = 13 m) (see legend). The CTD+jetski sampling period (1200 to 1500 h, Fig. 4) is indicated by the gray bar between vertical dashed lines.

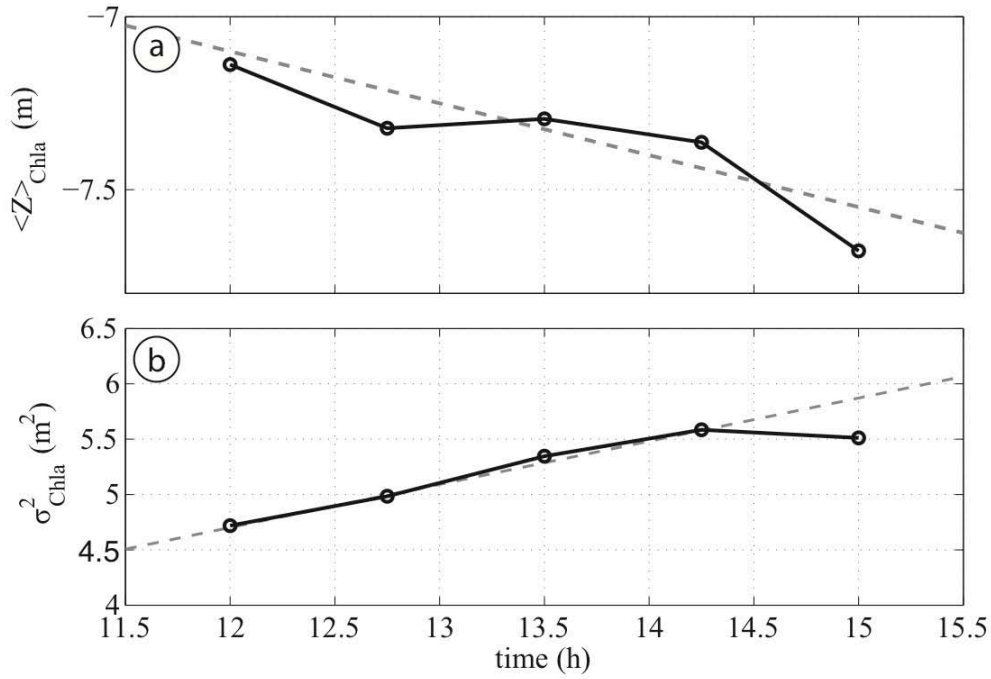

Figure 12. Time series from 1130 to 1530 h on 12 Oct based upon the CTD+Chl *a* surveys (between H = 5 to 12 m depth, see Fig. 4) of (a) depth $\langle z \rangle_{Chla}$ of the center of mass of cross-shore averaged $\langle$Chl *a* $(z)\rangle$ and (b) squared half-width σ^2_{Chla} (eq. 4) of the Chl $a(z)$ layer. In (a), the linear best fit (dashed line) yields a downward velocity of 60 μms^{-1} and in (b) the linear best fit (over the first four data points, dashed line) gives a Chl $a(z)$ vertical diffusivity $\kappa_{zz} \sim 0.5 \times 10^{-4}$ m^{2}s^{-1}.

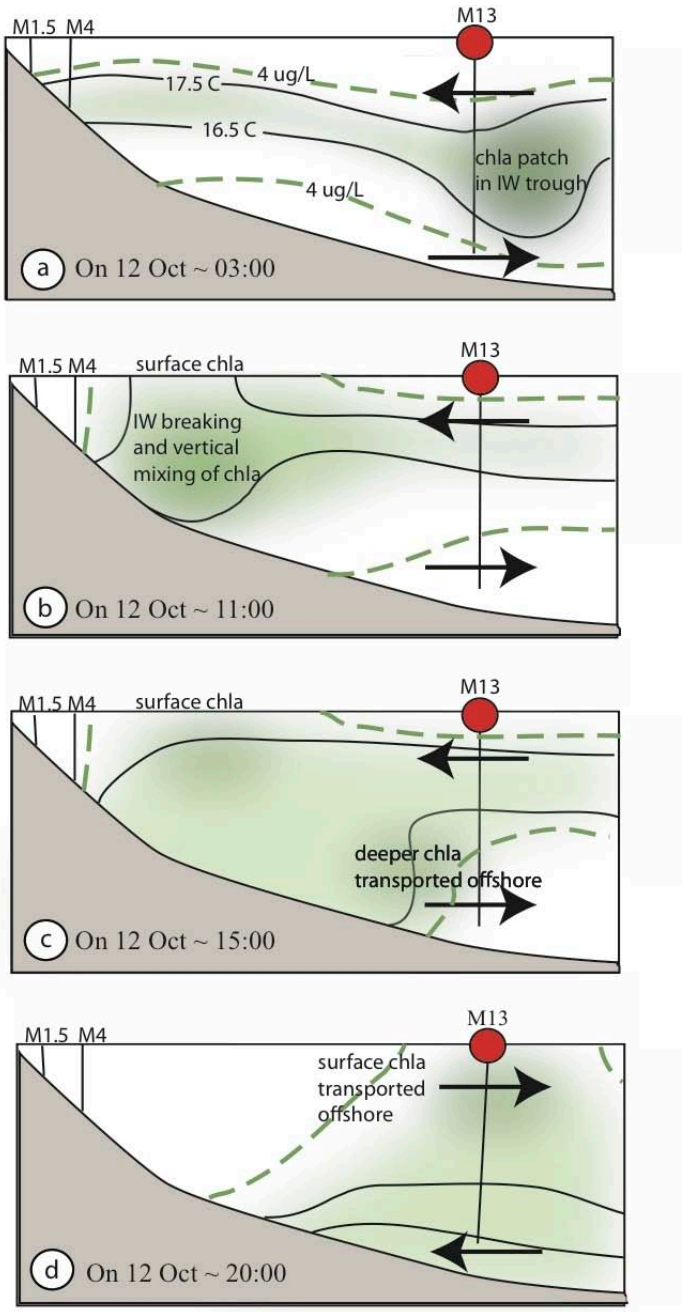

Figure 13. Schematic summarizing the 12 Oct 2006 observations. The locations of M13 (red circle w/ vertical line, 1 km from shore, H = 13 m) and the M1.5 and M4 frames are indicated (see triangles with vertical lines, Fig. 2). Jetski and CTD+Chl *a* casts provided additional observations. (a) Chl *a* in an sIW trough was locally concentrated by swimming and sIW strain as the wave propagated onshore, (b) sIW breaking in shallow water caused vertical mixing and outcropping of the 17.5 °C isotherm and upper portion of the Chl *a* patch, (c) deeper Chl *a* was advected offshore with the near-bottom baroclinic currents and (d) surface Chl *a* is advected offshore after the reversal of the baroclinic currents.